Femtosecond laser-induced modification at aluminum/diamond interface

Tatsuya Okada[1]*, Takuro Tomita[1], Tomoyuki Ueki[1], Yuki Masai[2], Yota Bando[2], and Yasuhiro Tanaka[3]

[1]*Graduate School of Science and Technology, Tokushima University, Tokushima 770-8506, Japan*

[2]*Graduate Student, Graduate School of Advanced Technology and Science, Tokushima University, Tokushima 770-8506, Japan*

[3]*Department of Advanced Materials Science, Faculty of Engineering, Kagawa University, Takamatsu 761-0396, Japan*

*E-mail: tatsuya-okada@tokushima-u.ac.jp

We investigated femtosecond-laser-induced modification at an Al/diamond interface. The interface was irradiated from the backside through the diamond substrate, which is transparent to the laser beam. Extremely high pulse energies, i.e., 200 and 100 μJ/pulse, were used to irradiate the interface. The cross-section of the laser-irradiated line was observed with conventional and high-voltage transmission electron microscopy. The modification of the laser-irradiated interface was characterized by the formation of an amorphous phase sandwiched between the deformed Al film and the diamond substrate. The major chemical component of the amorphous phase was identified as carbon, blown from the diamond substrate. The newly formed interface between the amorphous phase and the diamond substrate was concave. In addition, a fine ripple structure with an average spacing one-quarter

the wavelength of the laser light was formed only in the sample irradiated by the higher-energy pulses.

1. Introduction

Diamond is applied to cutting tools, heatsinks and high-power laser windows owing to its hardness, thermal conductivity and transparency, and is also known as a wide-bandgap semiconductor having a bandgap as large as 5.5 eV. Compared to other well-known wide-bandgap semiconductors such as silicon carbide (SiC) and gallium nitride (GaN), diamond has a three to four times higher breakdown electric field and 1.5 times higher carrier mobility.[1)] These superior properties make diamond a candidate for high-voltage, high-temperature, and high-frequency devices.[2-6)] However, before practical diamond-based power devices can be fabricated, many technological problems remain to be solved. One has to do with the difficulty in surface processing; e.g., processing by conventional machining or etching is practically impossible. Another problem is related to the difficulty in introducing foreign atoms into diamond. Hence, contact formation and local doping become technological challenges.

In recent years, femtosecond lasers have been attracting attention as a tool for inducing surface or interior modification of materials. A femtosecond laser is an ultra-short pulse laser having a typical pulse duration of about 100 fs. It can introduce high-density energy (~10^9 J/cm^3) into a small volume (~1 μm^3) in a very short time. Unlike other types of lasers such as nanosecond or continuous wave lasers, the thermal diffusion associated with irradiation is so small as to be practically negligible. Even in diamonds having the highest thermal

conductivity among all solid materials, the thermal diffusion length is estimated to be on the order of 10 nm, two orders of magnitude smaller than the minimum processing size (~1 μm) by femtosecond laser.

Femtosecond laser irradiation on a solid surface could induce Coulomb explosion, which results in cutting, removal, deformation and modification of the surface. Such a phenomenon is referred to as laser ablation.[7] It is known that when laser fluence is around the ablation threshold, laser-induced periodic surface structures (LIPSS), also described as “ripples”, are formed.[8] Fine ripple structures having periods several times shorter than the wavelength of laser light have been attracting much attention[9-11] because their formation cannot be simply attributed to interference between the incident and scattered light at the surface.[12-19] From a practical viewpoint, fine rippling is also of interest because it is potentially applicable to fine surface processing. When a femtosecond laser is irradiated into the interior of a transparent material, a Coulomb explosion is confined inside the material, which results in pronounced and periodic changes in physical and chemical properties of the irradiated region.

Several research groups have reported on the femtosecond laser ablation of diamond.[20-28] Hsu et al. carried out systematic experiments on femtosecond laser irradiation, both on the surface and in the interior of diamond single crystals.[26] They reported high- and low-frequency surface LIPSS formation for both stationary and translated samples. For the interior irradiation, they found the formation of a subwavelength periodic structure at the

position where the irradiated line met the side surface of the diamond crystal.

We have been studying the modification of the metal/semiconductor interface by directly irradiating the interface through the transparent semiconductor.[29,30] When the interface between nickel (Ni) and SiC was irradiated by a femtosecond laser from the SiC side, high-density defects were introduced in the SiC crystal adjacent to the interface. Post-irradiation annealing at 573 to 723 K induced diffusion of Ni, Si and C atoms in the defected region. These annealing temperatures were lower than those used for conventional annealing, 1073 K or higher, for contact formation.[31] Therefore, laser-induced crystallographic defects assisted atomic diffusion at relatively low temperatures. This defect-assisted diffusion may become a new approach to fabricating ohmic contacts at the Ni/SiC interface. We intend to apply this technique to metal/diamond interfaces. If foreign atoms are successfully introduced into a diamond single crystal, this technique will be applicable not only to ohmic contact formation but also to local doping, neither of which is easy using the existing diamond technologies.

At present, we are studying femtosecond-laser-induced modification at the metal/diamond interface before pursuing our final goal, i.e., application of defect-assisted diffusion to contact formation and local doping in the metal/diamond system. Special attention is paid to the morphology, crystal structure and chemical composition of the modified region because they are critically important in defect-assisted diffusion.[29,30] In the

present study, the interface between an aluminum (Al) film and a single-crystalline diamond substrate was irradiated from the backside, through a diamond single-crystal, by a femtosecond laser. We explored an extremely high fluence range, i.e., 0.5 and 1 kJ/cm^2, three orders of magnitude higher than in previous studies.[26] In the subsequent microstructural studies using cross-sectional transmission electron microscopy (TEM), we found two different morphologies at the interface, i.e., a concave interface with and without periodic fine ripple structures. The microstructural analyses of the crystal structure and chemical composition of the modified region are also reported in the present paper.

2. Experimental procedure

The diamond single-crystals grown by chemical vapor deposition were purchased from EDP and were used as substrates. The diamond was classified as IIa type based on its almost complete transparency to infrared. The crystal was 3×3×0.3 mm^3 in size and had a polished (001) surface with an average roughness (R_a) less than 5 nm. The edges of the crystal were along <100> directions perpendicular to the [001] direction. Prior to Al deposition, the crystal was ultrasonically cleaned in acetone, ethanol and distilled water. An Al thin film was deposited on the diamond substrate in a vacuum (< 5.0×10^{-3} Pa) using an ULVAC VPC-061 deposition apparatus. Two samples with different Al film thicknesses were prepared, i.e., 200 nm and 500 nm for Samples 1 and 2, respectively.

The laser light was focused on the Al/diamond interface through the transparent diamond substrate. In general, such irradiation is referred to as back-side irradiation. The light source was a Ti:sapphire regenerative amplifier at 1 kHz based on a chirped pulse amplification system operating at 800 nm (Spectra-Physics Spitfire). Prior to the irradiation, the sample was placed on a stage so that fine tilting was possible, and we confirmed that the focus was constant in an area ten times larger than the irradiation area (1.5×1.5 mm^2). The irradiation was made drawing a zig-zag pattern at a scan speed of 50 μm/s on the Al/diamond interface as schematically shown in Fig. 1. The spacing between major irradiation lines was 5 μm and 100 μm for Samples 1 and 2, respectively. The electric field of laser light was parallel to the major lines. The wavelength, duration and frequency of the laser pulse were 800 nm, 130 fs, and 1 kHz, respectively. The pulse energies were 200 μJ/pulse and 100 μJ/pulse for Samples 1 and 2, respectively. Since the beam profile was assumed to be Gaussian, we evaluated the beam diameter using the D^2 method. The diameter of the laser beam at the Al/diamond interface was about 4.6 μm, so that the laser fluences were about 1 kJ/cm^2 (200 μJ/pulse) and 0.5 kJ/cm^2 (100 μJ/pulse), including the 20% reflection loss at the interface. The Al film thickness, laser energy and irradiation line spacing for Samples 1 and 2 are summarized in Table I.

TEM sample preparation to observe the cross section of the laser-irradiated line was carried out by a pick-up technique using Ga^+ focused ion beam (FIB) micro-machining. An FEI Quanta 3D 200i equipped with an Omniprobe pick-up system was used. Due to the

explosive reaction at the laser-irradiated interface, the surface above the irradiated line was deformed. A rectangular protective film of platinum (Pt) alloy was first deposited on the deformed region. Deep trenches (25×20 μm^2 on the surface with a tapered bottom) were made on both sides of the protective film, leaving a 2-μm-thick wall between the trenches. The three sides of the wall were cut, leaving a small volume at one of the upper corners. A sharp probe was made closer to the other corner and the probe tip was welded to the wall. Then the left volume was cut and a piece of 10×5×2 μm^3 was picked up. The piece was welded to a pillar of a sample grid. The connection between the probe and the piece was cut. Finally, the piece was thinned until an electron transparent thickness (~100 nm) was obtained.

A JEOL JEM-2100F operated at 200 kV was used to observe the microstructure of the irradiated interface in a scanning transmission electron microscopy (STEM) mode. A selected area diffraction pattern (SADP) was taken to obtain crystallographic information of the laser-modified region. To observe elemental distribution at the interface region, a high-voltage electron microscope (HVEM) JEOL JEM-1300NEF at Kyushu University equipped with an in-column Ω-filter electron energy loss spectroscopy (EELS) system was operated at 1250 kV.

3. Results and discussion

3.1 As-deposited state

The as-deposited samples had a smooth and featureless surface, irrespective of the

thickness of the Al film. A cross-sectional TEM sample was prepared from Sample 1. A carbon (C) map was reconstructed from the HVEM/EELS data, as shown in Fig. 2. In the map, the high-C-concentration area appears bright. Hence, the bright diamond substrate contrasts sharply with the dark Al film. The flat Al/diamond interface is clearly visible. The intermediate brightness of the protective film reflects the fact that the protective film is not pure Pt but a C-containing Pt alloy.

3.2 Sample 1 after irradiation (200 μJ/pulse)

An optical micrograph of the Al film surface after the back-side irradiation is shown in Fig. 3. The irradiated area appears darker than the surrounding area. As will be described in this section, this is due to the carbon atoms blown from the diamond substrate through the partially broken Al film to reach the surface. A cross-sectional TEM sample was prepared from the area indicated by the circular symbol in Fig. 3.

Figure 4(a) is a STEM dark-field image of the laser-modified area and its schematic diagram. The capping Al film is severely deformed and a large concavity is formed in the center. The area between the capping Al film and the diamond substrate appears dark. In general, the area of lower density appears darker in the STEM dark-field image. Therefore, the contrast suggests that the sandwiched area has a lower density than the crystalline diamond. The interface between the substrate and the dark area sags downwards in the center

with very fine periodic undulations, although the spacing between neighboring peaks is not constant. Since six peaks exist in a distance of 970 nm, the average spacing is estimated to be about 200 nm, and this value is one-quarter of the wavelength of the laser light (800 nm). The morphological features are similar to the fine surface ripples observed in femtosecond-laser-irradiated diamond.[26] In the following, the fine periodic undulations are referred to as interface ripples. An SADP taken from the dark area [a circular symbol in Fig. 4(a)] is shown in Fig. 4(b). No crystalline spot pattern is observed but only a "halo" ring characteristic of the amorphous phase. The SADP clearly shows that the dark area just above the interface ripples is amorphized by the laser irradiation.

HVEM/EELS analyses were carried out to visualize the elemental distribution in the laser-modified region. Figure 5(a) is a "zero-loss" image of the analyzed area, reconstructed from transparent electrons with no energy loss—that is, elastically scattered electrons. Since most of the inelastically scattered electrons were removed from the zero-loss signals, a high-contrast image with weak background was obtained. Panels (b) and (c) in Fig. 5 are elemental maps of C and Al, respectively. Compared with the C mapping of the as-deposited state (Fig. 2), the interface ripples are clearly visible. In addition, a cloud-like contrast of the C distribution against a dark background is also recognized. The existence of C atoms above the interface ripples corresponds to the blown C atoms from the diamond substrate. A close look at the C distribution in Fig. 5(b) demonstrates that C exists even outside the interface

ripples. This suggests that in the periphery of a laser beam with a Gaussian energy distribution, the local fluence is higher than the threshold for laser ablation but lower than that for ripple formation. The fine features of the C distribution are not visible in the TEM/energy dispersive X-ray (EDX) spectroscopy mapping because the sensitivity to light elements is lower than that in EELS. In addition, EELS signal intensity is very sensitive to the sample thickness. An EELS system equipped with a TEM operated at 200 kV or lower requires extremely thin samples, much thinner than 100 nm, to clearly resolve C signals. Hence, the C distribution data obtained from the present samples with moderate thickness (~100 nm thick) are only made possible by the EELS system combined with an HVEM operated at 1250 kV.

The distributions of C [Fig. 5(b)] and Al [Fig. 5(c)] appear almost complementary to each other. In some areas, the Al film is discontinuous and C is found in the crack of the Al film. This is accounted for by the fact that the explosive reaction at the Al/diamond interface broke the Al film and C atoms from the diamond were blown through the crack to reach the film surface. Presumably, C is the major component of the amorphous phase sandwiched by the partially broken Al film and the diamond substrate. There is a small area in which C and Al appear to coexist. This might be attributable to high-speed intrusions of C atoms blown into the Al film. Further study is needed to clarify this issue.

3.3 Sample 2 after irradiation (100 μJ/pulse)

As shown in Fig. 6, the surface undulation of Sample 2 after the back-side laser irradiation was less pronounced than that of Sample 1 due to the thicker Al film and lower pulse energy. A cross-sectional TEM sample was prepared from the area indicated by the circular symbol in Fig. 6.

A STEM dark-field image of the laser-modified area is shown in Fig. 7(a). Although the Al capping film is deformed, no large surface cavity as in Sample 1 [Fig. 4(a)] was found. Figure 7(b) is an SADP taken from the dark area between the Al film and diamond substrate as shown by a circular symbol in Fig. 7(a). Amorphization of the sandwiched area is clearly recognized from the halo rings in the SADP. The formation mechanisms of the amorphized area appear identical to those of Sample 1. The interface between the dark area and diamond substrate sags downwards in the center, but with no clear ripples.

In order to check the chemical reactivity of the laser-modified region, Sample 2 was chemically etched in aqua regia. A post-etching optical micrograph is shown in Fig. 8. As a result of complete dissolution of the Al film, a dark zig-zag pattern that was not seen in the as-irradiated state (Fig. 6) is clearly visible. The dark pattern agrees exactly with the laser-irradiation pattern traced on the Al/diamond interface. Considering the chemical inertness to aqua regia, it was concluded that the dark zig-zag pattern in Fig. 8 originated from the laser-induced amorphous C phase formed between the capping Al film and the diamond substrate.

4. Summary

The Al/diamond interface was back-side irradiated through the transparent diamond substrate with femtosecond laser pulses in a zig-zag pattern. Pulse fluences were three orders of magnitude higher than in the previous studies for surface or internal irradiation. The cross section of the laser-modified region at the interface was examined with TEM/SADP and HVEM/EELS techniques. In the sample irradiated with 1 kJ/cm^2, fine ripples were formed with an average spacing of 200 nm. The amorphous phase above the fine ripples mainly consists of C atoms blown from the diamond substrate. In the sample irradiated with 0.5 kJ/cm^2, there was a laser-induced concavity at the interface and amorphous phase, but no fine ripples were found.

Acknowledgments

This work was partly supported by Advanced Characterization Platform of the Nanotechnology Platform Japan sponsored by the Ministry of Education, Culture, Sports, Science and Technology (MEXT). We are grateful for the technical assistance provided by the Ultramicroscopy Research Center, Kyushu University. Financial support by JSPS KAKENHI Grant-in-Aid for Fundamental Research (C), Grant Number 15K06466, is also acknowledged.

References

1) M. I. Landstrass, M. A. Plano, M. A. Moreno, S. McWilliams, L. S. Pan, D. R. Kania, and S. Han, Diamond Relat. Mater. **2**, 1033 (1993).
2) A. Aleksov, A. Denisenko, M. Kunze, A. Vescan, A. Bergmaier, G. Dollinger, W. Ebert, and E. Kohn, Semicond. Sci. Technol. **18**, S59 (2003).
3) J. E. Butler, M. W. Geis, K. E. Krohn, J. Lawless Jr., S. Deneault, T. M. Lyszczarz, D. Flechtner, and R. Wright, Semicond. Sci. Technol. **18**, S67 (2003).
4) H. Umezawa, M. Nagase, Y. Kato, and S. Shikata, Diamond Relat. Mater. **24**, 201 (2012).
5) T. Iwasaki, J. Yaita, H. Kato, T. Makino, M. Ogura, D. Takeuchi, H. Okushi, S. Yamasaki, and M. Hatano, IEEE Electron Device Lett. **35**, 241 (2014).
6) P-N. Volpe,P. Muret, J. Pernot, F. Omnès, T. Teraji, Y. Koide, F. Jomard, D. Planson, P. Brosselard, N. Dheilly, B. Vergne, and S. Scharnholz, Appl. Phys. Lett. **97**, 223501 (2010).
7) N. M. Bulgakova, R. Stoian, A. Rosenfeld, I. V. Hertel, and E. E. B. Campbell, in *Laser Ablation and its Application*, ed. C. Phipps (Springer, New York, 2007), p. 17.
8) M. Birnbaum, J. Appl. Phys. **36**, 3688 (1965).
9) N. Yasumaru, K. Miyazaki, and J. Kiuchi, Appl. Phys. A **76**, 983 (2003).
10) A. Borowiec and H. K. Haugen, Appl. Phys. Lett. **82**, 4462 (2003).
11) P. Rudolph and W. Kautek, Thin Solid Films **453-454**, 537 (2004).
12) J. E. Sipe, J. F. Young, J. S. Preston, and H. M. van Driel, Phys. Rev. B **27**, 1141 (1983).
13) J. F. Young, J. S. Preston, H. M. van Driel, and J. E. Sipe, Phys. Rev. B **27**, 1155 (1983).
14) J. F. Young, J. E. Sipe, and H. M. van Driel, Phys. Rev. B **30**, 2001 (1984).
15) G. Miyaji and K. Miyazaki, Appl. Phys. Lett. **91**, 123102 (2007).
16) G. Miyaji and K. Miyazaki, Opt. Express **16**, 16265 (2008).
17) J. Reif, O. Varlamova, and F. Costache, Appl. Phys. A **92**, 1019 (2008).
18) J. Reif, F. Costache, O. Varlamova, G. Jia, and M. Ratzke, Phys. Status Solidi (C) **6**, 681 (2009).

19) S. Sakabe, M. Hashida, S. Tokita, S. Namba, and K. Okamuro, Phys. Rev. B **79**, 033409 (2009).

20) P. Tosin, A. Blatter, and W. Lüthy, J. Appl. Phys. **78**, 3797 (1995).

21) A. M. Ozkan, A. P. Malshe, T. A. Railkar, W. D. Brown, M. D. Shirk, and P. A. Molian, Appl. Phys. Lett. **75**, 3716 (1999).

22) Q. Wu, Y. Ma, R. Fang, Y. Liao, Q. Yu, X. Chen, and K. Wang, Appl. Phys. Lett. **82**, 1703 (2003).

23) A. Malshe and D. Deshpande, J. Mater. Process. Technol. **149**, 585 (2004).

24) M. Huang, F. Zhao, Y. Cheng, N. Xu, and Z. Xu, Phys. Rev. B **79**, 125436 (2009).

25) M. Shinoda, R. R. Gattass, and E. Mazur, J. Appl. Phys. **105**, 053102 (2009).

26) E. M. Hsu, N. A. Mailman, G. A. Botton, and H. K. Haugen, Appl. Phys. A **103**, 185 (2011).

27) S. Su, J. Li, G. C. B. Lee, K. Sugden, D. Webb, and H. Ye, Appl. Phys. Lett. **102**, 23913 (2013).

28) P. Calvani, A. Bellucci, M. Girolami, S. Orlando, V. Valentini, A. Lettino, and D. M. Trucchi, Appl. Phys. A **117**, 25 (2014).

29) T. Ueki, K. Morimoto, H. Yokota, T. Tomita, and T. Okada, Appl. Phys. Express **8**, 026503 (2015).

30) Y. Takidani, K. Morimoto, K. Kondo, T. Ueki, T. Tomita, Y. Tanaka, and T. Okada, J. Laser Micro/Nanoeng. **10**, 314 (2015).

31) I. P. Nikitina, K. V. Vassilevski, N. G. Wright, A. B. Horsfall, A. G. O'Neill, and C. M. Johnson, J. Appl. Phys. **97**, 083709 (2005).

Fig. 1. Schematic diagram of laser irradiation. The laser light is focused at the Al/diamond interface through the transparent diamond single crystal. The electric field (***E***) is parallel to the major irradiation line. Cross-sectional TEM observations are made in the direction parallel to the major irradiation line.

Fig. 2. C mapping of the as-deposited state of Sample 1, reconstructed from HVEM/EELS data. The areas with high C concentrations appear bright.

Fig. 3. Optical micrograph of the Al film surface after back-side laser irradiation (Sample 1). A cross-sectional TEM sample was prepared from the circular area.

Fig. 4. (a) STEM dark-field image and a schematic diagram of the laser-modified area in Sample 1. (b) SADP taken from the circle in (a).

Fig. 5. (a) Zero-loss image reconstructed from HVEM/EELS signals. The distributions of C and Al reconstructed from EELS data are shown in (b) and (c), respectively.

Fig. 6. Optical micrograph of the Al film surface after back-side laser irradiation (Sample 2). A cross-sectional TEM sample was prepared from the circular area.

Fig. 7 (a) STEM dark-field image of the laser-modified area in Sample 2. (b) SADP taken from the circle in (a).

Fig. 8. Optical micrograph of the (001) surface of Sample 2 after removing Al film by chemical etching in aqua regia.

Table I. Al film thickness, laser energy, and irradiation line spacing for the samples.

	Al film thickness	Laser energy	Irradiation line spacing
Sample 1	200 nm	200 μJ/pulse (1 kJ/cm^2)	5 μm
Sample 2	500 nm	100 μJ/pulse (0.5 kJ/cm^2)	100 μm

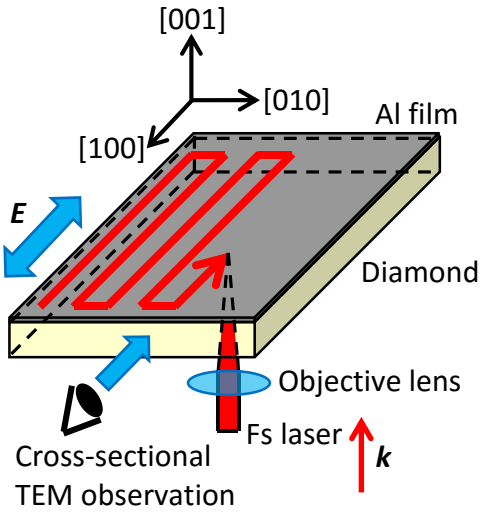

Fig. 1 (Color online)

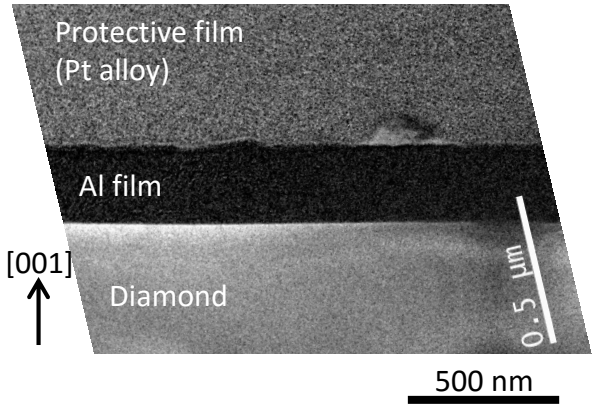

Fig. 2 (Black and white)

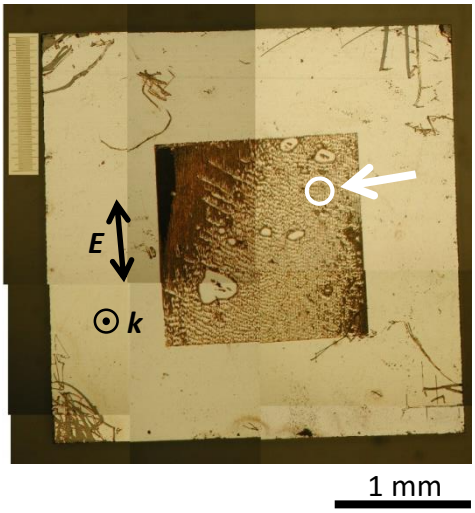

Fig. 3 (Color online)

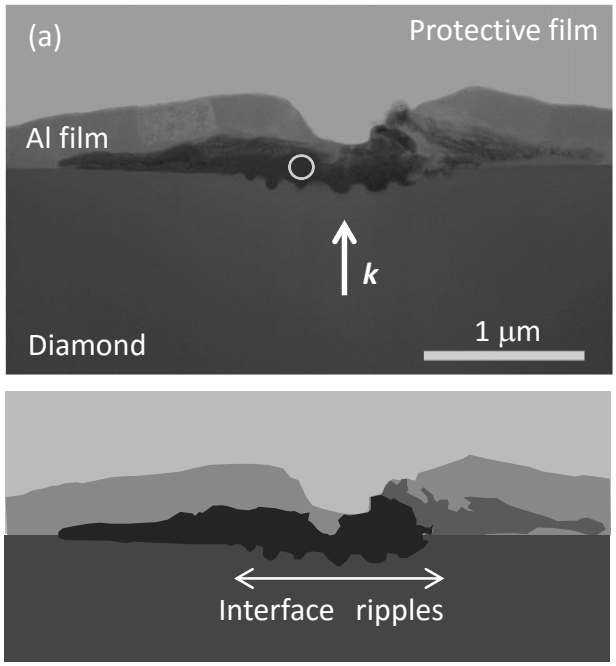

Fig. 4 (Black and white)

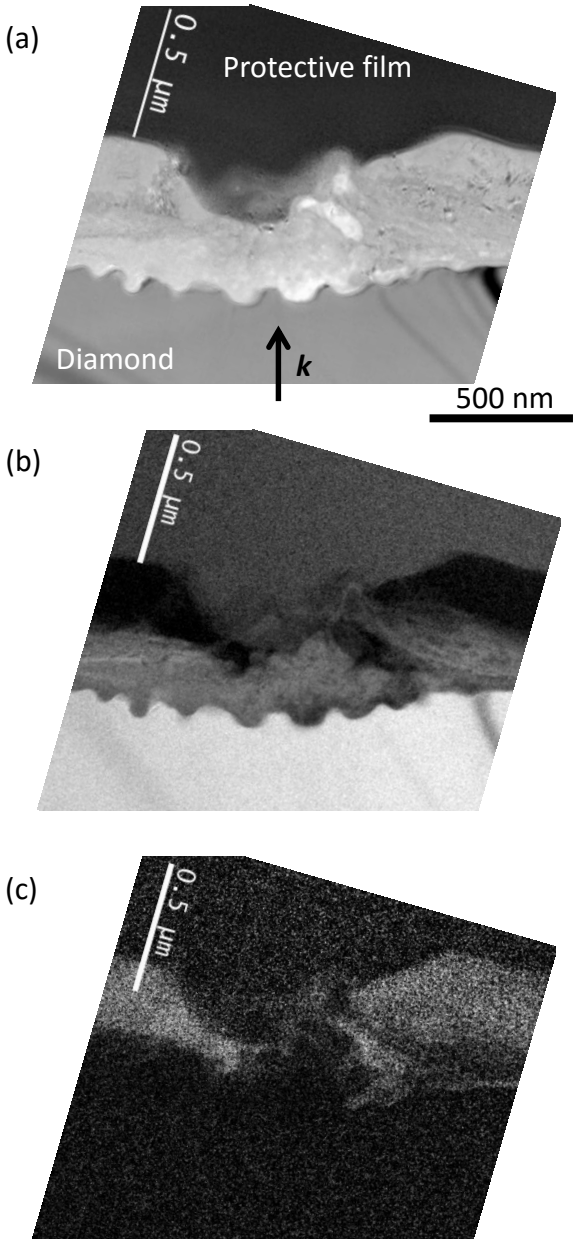

Fig. 5 (Black and white)

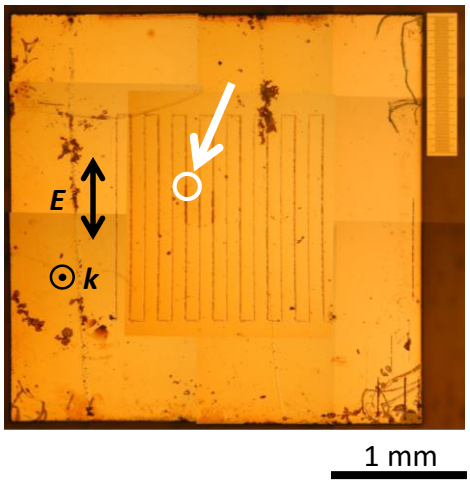

Fig. 6 (Color online)

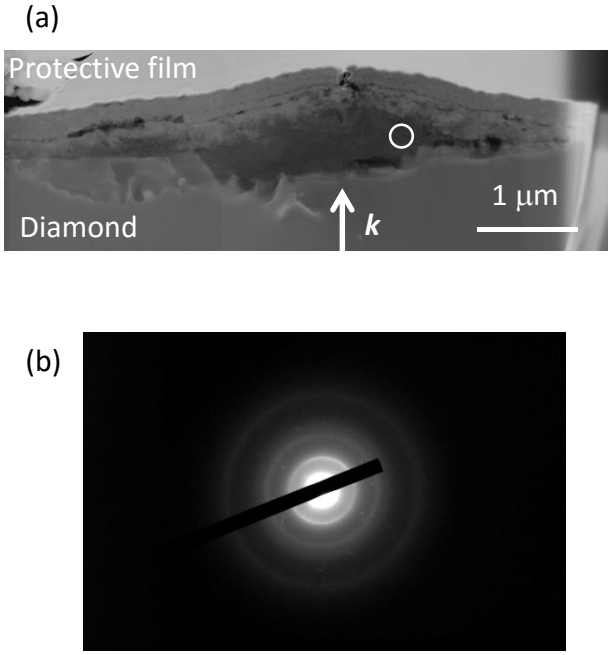

Fig. 7 (Black and white)

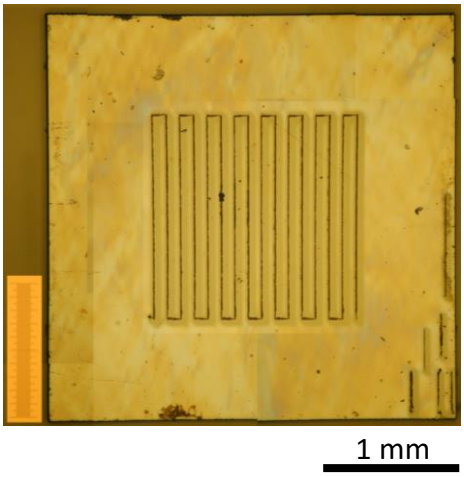

Fig. 8 (Color online)